

Pressure effect on magnetism and valence in ferromagnetic superconductor $\text{Eu}(\text{Fe}_{0.75}\text{Ru}_{0.25})_2\text{As}_2$

Zachary Nix¹, Jiyong Zhao², Esen E Alp², Yuming Xiao³, Dongzhou Zhang⁴, Guang-Han Cao⁵ , Yogesh K Vohra¹  and Wenli Bi^{1,*} 

¹ Department of Physics, University of Alabama at Birmingham, Birmingham, AL 35294, United States of America

² Advanced Photon Source, Argonne National Laboratory, Argonne, IL 60439, United States of America

³ HPCAT, X-ray Science Division, Argonne National Laboratory, Argonne, IL 60439, United States of America

⁴ Hawaii Institute of Geophysics and Planetology, School of Ocean and Earth Science and Technology, University of Hawaii at Manoa, Honolulu, HI 96822, United States of America

⁵ School of Physics, Zhejiang University, Hangzhou 310027, People's Republic of China

E-mail: wbi@uab.edu

Received 13 April 2022, revised 11 July 2022

Accepted for publication 27 July 2022

Published 4 August 2022



CrossMark

Abstract

$\text{Eu}(\text{Fe}_{0.75}\text{Ru}_{0.25})_2\text{As}_2$ is an intriguing system with unusual coexistence of superconductivity and ferromagnetism, providing a unique platform to study the nature of such coexistence. To establish a magnetic phase diagram, time-domain synchrotron Mössbauer experiments in ^{151}Eu have been performed on a single crystalline $\text{Eu}(\text{Fe}_{0.75}\text{Ru}_{0.25})_2\text{As}_2$ sample under hydrostatic pressures and at low temperatures. Upon compression the magnetic ordering temperature increases sharply from 20 K at ambient pressure, reaching ~ 49 K at 10.1 GPa. With further compression, the magnetic order is suppressed and eventually collapses. Isomer shift values from Mössbauer measurements and x-ray absorption spectroscopy data at Eu L_3 edge show that pressure drives Eu ions to a homogeneous intermediate valence state with mean valence of ~ 2.4 at 27.4 GPa, possibly responsible for the suppression of magnetism. Synchrotron powder x-ray diffraction experiment reveals a tetragonal to collapsed-tetragonal structural transition around 5 GPa, a lower transition pressure than in the parent compound. These results provide guidance to further work investigating the interplay of superconductivity and magnetism.

Keywords: iron pnictide, magnetism, pressure, synchrotron spectroscopy

(Some figures may appear in colour only in the online journal)

1. Introduction

Superconductivity and magnetism are two intriguing collective phenomena which are traditionally thought to be incompatible and mutually competitive. Surprisingly, these

conventionally competitive phenomena have been found to coexist in few systems such as heavy fermions [1–3]. Rare earth-based iron pnictide superconductors have recently emerged as a research focus in condensed matter physics due to the peculiar coexistence of robust superconductivity and strong local moment magnetism from 4*f* electrons [4–11]. Among them Eu-based iron pnictide superconductors are the latest outstanding example of completely paradigmatic

* Author to whom any correspondence should be addressed.

materials [12]. These compounds adopt a layered structure with superconductivity originating from the Fe-As layers and a strong local magnetic moment ($7 \mu_B$) from the Eu layers. Compared to other magnetic superconductors such as heavy fermion systems, they exhibit much higher superconducting critical temperatures $T_c \sim 30$ K) and magnetic ordering temperatures (T_o) similar to T_c . The more accessible critical temperatures in $\text{Eu}(\text{Fe}_{0.75}\text{Ru}_{0.25})_2\text{As}_2$ make it experimentally feasible to study the correlation of superconductivity and magnetism with standard cryogenic setup. Previous studies have claimed that the interaction between the Eu magnetic and Fe-As superconducting layers is rather weak [13, 14]. However, microscopic studies such as Mössbauer experiments have found a sizable transferred magnetic field in the Fe sublattice by the rare earth ions, suggesting an intriguing interplay between the local magnetism and superconductivity [15–17].

Eu-based iron pnictides exhibit extremely rich phenomena including spin-density-wave (SDW), superconducting ground state, and strong local moment magnetism from divalent Eu ions ($4f^7$). Non-superconducting parent compounds such as EuFe_2As_2 , SrFe_2As_2 , and BaFe_2As_2 undergo tetragonal to orthorhombic structural phase transition associated with SDW order in the Fe sublattice [18–20]. In EuFe_2As_2 with pressure application, the SDW order is suppressed and superconductivity emerges [21–23]. At higher pressure a tetragonal to collapsed-tetragonal transition linked to Eu magnetic transition has been observed [24, 25]. In addition, due to proximity of $\text{Eu}^{2+}(4f^7, J = 7/2)$ and $\text{Eu}^{3+}(4f^6, J = 0)$ energy levels, the valence state of Eu can be tuned by external parameters (pressure, temperature, and magnetic field) in many Eu-intermetallic compounds such as EuM_2Ge_2 ($M = \text{Ni, Pd, Pt}$) and EuNi_2P_2 [26–28]. As a consequence of the valence transition, the local moment magnetism is weakened and eventually suppressed completely due to the Van Vleck nature of $4f^6$. Therefore, to understand magnetic behavior it is crucial to investigate the valence state simultaneously.

In this study we focus on evolution of the magnetic state, valence, and crystal structure of ferromagnetic superconductor $\text{Eu}(\text{Fe}_{0.75}\text{Ru}_{0.25})_2\text{As}_2$ under pressure. Previous studies in this system have shown anisotropic superconductivity below 23 K and magnetic order below 20 K from the Eu sublattice [29]. Conventional transmission Mössbauer and magnetization measurements have revealed a ferromagnetic component in the Eu magnetic state and absence of magnetic order in Fe sublattice with a weak transferred field from the Eu magnetic order. In addition, more recent neutron and theoretical studies have identified $\text{Eu}(\text{Fe}_{0.75}\text{Ru}_{0.25})_2\text{As}_2$ as a system of a three-dimensional anisotropic quantum Heisenberg model with universal critical exponent ($\beta = 0.385$) due to an enhanced Ruderman-Kittel-Kasuya-Yosida (RKKY) interaction between Eu atoms mediated by the more extended Ru $4d$ orbitals than the Fe $3d$ orbitals [30]. In this work, we have conducted experimental studies of magnetism, valence of Eu ions, and crystal structure in $\text{Eu}(\text{Fe}_{0.75}\text{Ru}_{0.25})_2\text{As}_2$ under pressure using time-domain synchrotron Mössbauer spectroscopy (SMS) in ^{151}Eu up to 27.4 GPa, partial-fluorescence-yield x-ray absorption spectroscopy (PFY-XAS) up to

38 GPa, and synchrotron powder x-ray diffraction (XRD) up to 12.4 GPa.

The rest of this paper is organized as follows. In section 2, a description of the three experimental methods (SMS, PFY-XAS, and XRD) used in this work is given. Section 3 presents the experimental results, including SMS studies up to 27.3 GPa with helium as pressure transmitting medium, PFY-XAS studies under compression up to 38 GPa as well as under decompression down to 1.5 GPa, and powder XRD results up to 12.4 GPa using methanol-ethanol (4:1) mixture as pressure medium. Pressure-induced changes in valence state of Eu estimated from isomer shift values are compared with the results from PFY-XAS data. By linking the magnetic order and mean valence under compression, possible origin of magnetism suppression is suggested. These high-pressure behaviors are compared with the experimental results in parent compound EuFe_2As_2 . Finally, section 4 presents a summary of this work.

2. Experimental methods

$\text{Eu}(\text{Fe}_{0.75}\text{Ru}_{0.25})_2\text{As}_2$ single crystals were grown from self-flux method [29] and the sample was previously characterized by electrical resistivity, magnetization, and conventional transmission Mössbauer experiments at low temperatures. High-pressure SMS experiments were carried out at Beamline 3ID at the Advanced Photon Source (APS), Argonne National Laboratory (ANL). Mössbauer spectroscopy is a sensitive technique for probing magnetism and electronic transitions on a microscopic scale. Thanks to the focused micron size beam, synchrotron-based time-domain Mössbauer spectroscopy has been applied widely in magnetic studies under high pressure [10, 31–34]. SMS experiments were conducted at the nuclear resonant energy of 21.54 keV for ^{151}Eu to investigate the magnetic transition in $\text{Eu}(\text{Fe}_{0.75}\text{Ru}_{0.25})_2\text{As}_2$. The synchrotron x-rays were focused to $15 \mu\text{m}$ (h) \times $15 \mu\text{m}$ (v) (full width at half maximum, FWHM). The experiments were performed during the standard 24-bunch timing mode of the APS with 153 ns separation between the two successive electron bunches allowing for data collection. This timing window is several lifetimes (14.1 ns) of the ^{151}Eu transition, allowing accurate determination of hyperfine parameters. A gas membrane-driven miniature panoramic diamond anvil cell was used in a specially designed helium-flow cryostat [35]. One pair of diamond anvils of 500 μm culet was used to generate pressure up to 27.4 GPa. Rhenium (Re) gasket was preindented to $\sim 80 \mu\text{m}$ and a hole of 250 μm was drilled using electric discharge machining (EDM) to form the sample chamber. A single crystalline $\text{Eu}(\text{Fe}_{0.75}\text{Ru}_{0.25})_2\text{As}_2$ sample was loaded in the gasket hole together with two ruby balls as in-situ pressure marker [36]. Helium was used as pressure transmitting medium. Information on the valence state of Eu ions was provided by measuring the isomer shift of ^{151}Eu using trivalent Eu_2O_3 (1.024 mm s^{-1} relative to EuF_3) as a reference sample [31]. Initial pressure was applied at room temperature during helium gas loading. Subsequent pressures were applied at 100 K. The SMS data were analyzed using the CONUSS

(coherent nuclear resonant scattering by single crystals) package [37].

To provide direct information on the valence of Eu and confirm the valence state derived from isomer shift measurements, PFY-XAS experiment at Eu L_3 edge (6.974 keV) was conducted at room temperature at Beamline 16ID-D of the APS, ANL. The x-rays were focused to 5 μm (FWHM). The incident x-ray energy was scanned from 6.954 keV to 7.024 keV. To avoid strong absorption by the diamond anvils, incoming x-rays traveled through a Be gasket and the fluorescence signal was collected. The signal was first analyzed with silicon analyzer and then collected with a Pilatus detector at 90 degree from the incident x-ray beam. Since the measurements were conducted in fluorescence mode, attenuation of fluorescence may occur as it travels out of the sample. Optimal sample position was determined by scanning the sample position to minimize this attenuation. High pressure was achieved using symmetric-type diamond anvil cell equipped with a pair of diamond anvils with 500 μm culet. A beryllium gasket was preindented to ~ 100 μm and a hole of 400 μm was drilled. Cubic boron nitride (cBN) and epoxy mixture was then filled in the gasket hole and indented to form the gasket insert in order to maintain a good sample thickness under pressure. A $\text{Eu}(\text{Fe}_{0.75}\text{Ru}_{0.25})_2\text{As}_2$ sample was loaded in the sample chamber formed by the cBN insert. Two ruby balls were loaded along with the sample and used as an in-situ pressure marker [36]. No pressure medium was used. Data was normalized in Athena, a part of the Demeter software package for XAS data processing and analysis [38]. Eu mean valence was obtained by modeling the XAS spectrum with two sets of Lorentzian and arctangent functions for divalent and trivalent states.

To study the high-pressure crystal structure, powder XRD experiment was carried out at room temperature on a powder $\text{Eu}(\text{Fe}_{0.75}\text{Ru}_{0.25})_2\text{As}_2$ sample ground from a single crystal at the 13BM-C Beamline (PX2) of the APS, ANL. An x-ray wavelength of 0.434 \AA was used. The x-ray beam was focused to 15 μm . High pressures up to 12.4 GPa were achieved using a BX-90 diamond anvil cell [39] equipped with a pair of Boehler-Almax anvils with culet of 500 μm diameter. A Re gasket was indented to 70 and a 250 μm hole was drilled with EDM to form the sample chamber. Methanol-ethanol 4:1 mixture was used as a hydrostatic pressure transmitting medium. Ruby was used as an in-situ pressure marker [36]. Image data was processed using Dioplas [40] and the resulting XRD spectra were analyzed using GSAS-II [41]. Structural data was obtained from Rietveld refinements.

3. Experimental results and discussion

3.1. SMS

SMS spectra at various pressure and temperature conditions are presented in figure 1. When the sample is cooled below the magnetic ordering temperature T_o , oscillations originating from magnetic hyperfine field (B_{hf}) and quadrupole splitting appear in the SMS data. At constant pressure, as the sample temperature is raised the oscillation frequency decreases due to the decrease of B_{hf} . When $\text{Eu}(\text{Fe}_{0.75}\text{Ru}_{0.25})_2\text{As}_2$ enters the

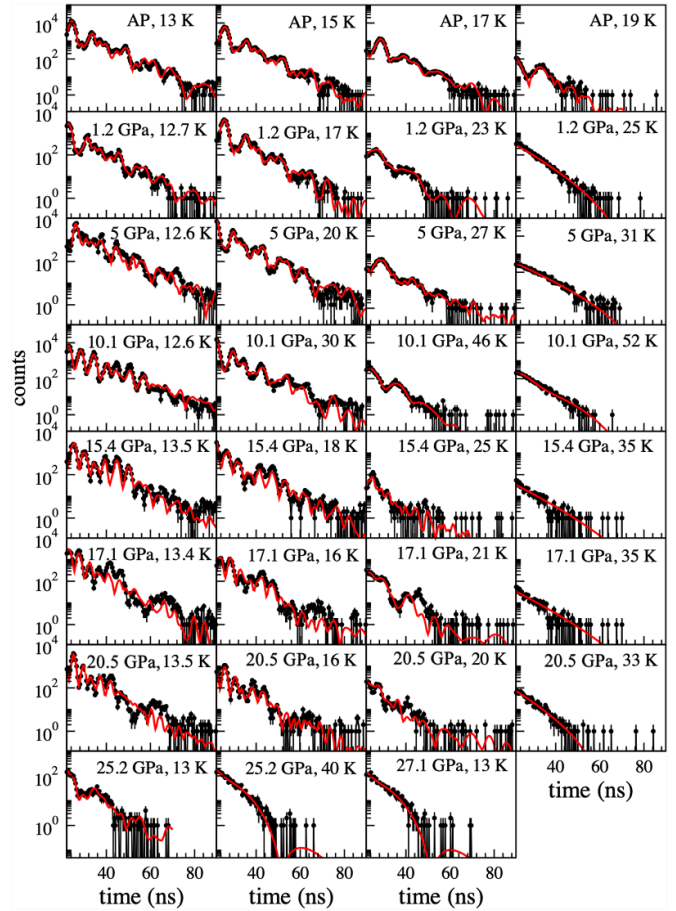


Figure 1. Selected ^{151}Eu SMS spectra of $\text{Eu}(\text{Fe}_{0.75}\text{Ru}_{0.25})_2\text{As}_2$ at high pressures and low temperatures. The black solid circles are experimental data. The errors are estimated random noise by taking the square root of the counts. Red lines are fits from CONUSS.

paramagnetic phase, the oscillations disappear, indicating no detectable quadrupole splitting in the paramagnetic phase. In addition, T_o is observed to increase initially and then decreases sharply with increasing pressure. At 27.1 GPa no magnetic order was observed down to 13 K. By modeling the SMS data hyperfine parameters, such as B_{hf} and quadrupole splitting can be extracted. The dependence of B_{hf} values with temperature at various pressures is plotted in figure 2. At ambient pressure and 13 K the extracted B_{hf} is 25.3 T, consistent with 28.8 T measured at 5 K from conventional Mössbauer spectroscopy [29]. And B_{hf} increases 49 T at 20.5 GPa and 13 K. In elemental Eu metal, a large increase of B_{hf} has also been observed under high pressure, which is likely due to an increase in polarization of conduction electrons by neighboring atoms [33]. To understand the enhanced B_{hf} of $\text{Eu}(\text{Fe}_{0.75}\text{Ru}_{0.25})_2\text{As}_2$, calculations of hyperfine parameters under pressure are warranted.

Additional SMS data were taken with Eu_2O_3 as reference to determine the change of isomer shift and provide information on Eu valence state. To simplify the time-domain spectra and data interpretation, data were taken at 100 K in the paramagnetic phase. The SMS data and simulated energy-domain spectra are shown in figure 3. At ambient pressure and 100 K the derived isomer shift is -11.8 mm s^{-1} , a typical value

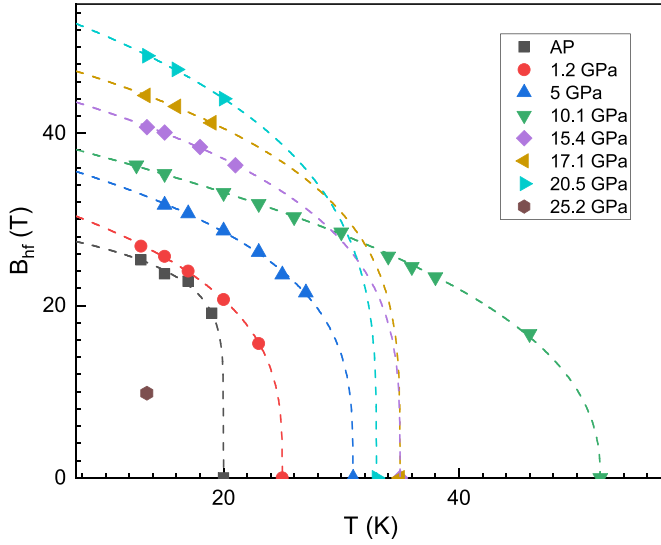


Figure 2. Magnetic hyperfine field of ^{151}Eu in $\text{Eu}(\text{Fe}_{0.75}\text{Ru}_{0.25})_2\text{As}_2$ as a function of temperature with increasing pressure from ambient pressure (AP) up to 25.2 GPa. The dashed lines serve as a guide to the eye.

for Eu^{2+} . This value is in good agreement with the reported -12.0 mm s^{-1} at 30 K [29]. As pressure is applied, the isomer shift of Eu increases continuously toward Eu^{3+} , reaching -5.8 mm s^{-1} at 27.4 GPa. At 17.7 GPa the signal from $\text{Eu}(\text{Fe}_{0.75}\text{Ru}_{0.25})_2\text{As}_2$ appears to decrease relative to the reference, likely due to a change in position on the reference, increasing the relative site ratio of Eu_2O_3 . It is noted that in the model for the paramagnetic SMS data from the sample, only one Eu site is needed, indicating that Eu ions take on homogeneous intermediate valence state under pressure on the time scale of Mössbauer measurements, in contrast to heterogeneous mixed valence case [42] where two Eu sites are needed to model the data. The hyperfine parameters are tabulated in table 1.

3.2. PFY-XAS

PFY-XAS data were taken under compression up to 38 GPa and then under decompression to 1.5 GPa. As shown in figure 4, Eu ions are in divalent state at 1.2 GPa evidenced by a single absorption peak above 6.974 keV which corresponds to $2p_{3/2}^6 4f^7 5d^0 6s^2 \rightarrow 2p_{3/2}^5 4f^7 5d^1 6s^2$ transition. As pressure is increased, a second absorption peak starts to appear at $\sim 8 \text{ eV}$ higher in energy, indicating a transition toward trivalent state corresponding to the transition $2p_{3/2}^6 4f^6 5d^1 6s^2 \rightarrow 2p_{3/2}^5 4f^6 5d^2 6s^2$. At higher pressure the Eu^{3+} peak intensity increases while Eu^{2+} intensity decreases, indicating a systematic increase of valence, consistent with the results from isomer shift measurements. When pressure is released, the divalent state of Eu ions is recovered, showing a reversible valence transition.

It is noted that in the intermediate valence state, the PFY-XAS data displays two distinct peaks, representing the divalent and trivalent states of Eu, while isomer shift data shows a

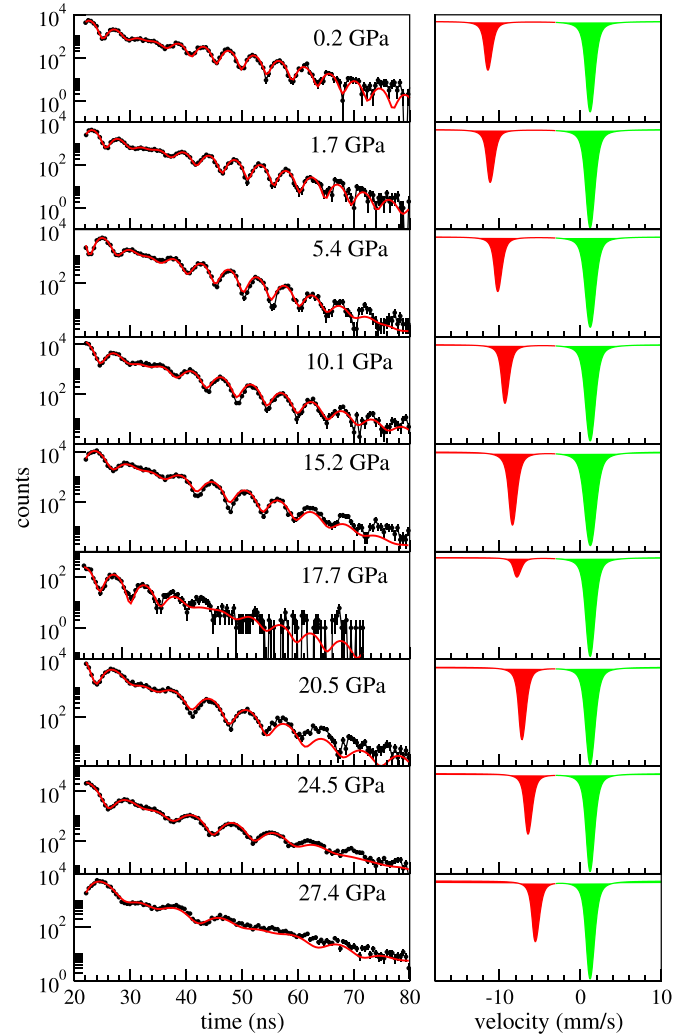


Figure 3. ^{151}Eu SMS spectra in $\text{Eu}(\text{Fe}_{0.75}\text{Ru}_{0.25})_2\text{As}_2$ at various pressures and 100 K along with Eu_2O_3 as reference located at ambient condition (left column) and corresponding simulations in energy domain (right column). In the energy-domain spectra shaded red lines are resonant absorption from $\text{Eu}(\text{Fe}_{0.75}\text{Ru}_{0.25})_2\text{As}_2$ and shaded green lines represent absorption from Eu_2O_3 .

single peak as seen in the simulated energy-domain Mössbauer spectra (figure 3). This observation originates from the different measurement time of the two techniques. Valence fluctuation between $4f^7$ and $4f^6$ configurations is typically on the order of 10^{-11} s [43]. The measurement time of XAS is $\sim 10^{-16} \text{ s}$ which is determined by the core hole lifetime. In the case of Mössbauer spectroscopy the typical time scale for measurement is $\sim 10^{-8} \text{ s}$. The measurement time of XAS is much shorter than the valence fluctuation rate and therefore two peaks are recorded. In contrast, only the average isomer shift from the intermediate valence state is observed by Mössbauer experiment due to the slow measurement time.

The mean valence of Eu is derived by modeling the PFY-XAS data with one set of Lorentzian and arctangent functions for each peak (figure 5). Assuming the relative occupancy of Eu^{2+} and Eu^{3+} states is proportional to the integrated area under each peak, the mean valence can be estimated and compared with the values from isomer shift measurements.

Table 1. List of B_{hf} , quadrupole splitting (Δ), and isomer shift (δ) of ^{151}Eu in $\text{Eu}(\text{Fe}_{0.75}\text{Ru}_{0.25})_2\text{As}_2$ at high pressure and various temperatures.

P (GPa)	T (K)	B_{hf} (T)	Δ (mm s^{-1})	δ (mm s^{-1})
0	13	25.31(3)	7.3(2)	
	15	23.75(2)	6.9(2)	
	17	22.82(4)	6.7(2)	
	19	19.15(6)	7.7(1)	
	100	0	0	-11.82(1)
0.5	100	0	0	-11.78(1)
1.2	12.7	26.70(4)	8.0(2)	
	15	25.69(3)	7.4(1)	
	17	23.92(4)	6.8(2)	
	20	20.70(6)	6.1(2)	
	23	15.57(6)	6.5(2)	
	25	0	0	
	100	0	0	-11.45(1)
5.0	15	31.56(5)	8.2(3)	
	17	30.65(3)	8.1(2)	
	20	28.66(4)	8.0(2)	
	23	26.23(3)	7.9(1)	
	25	23.61(3)	7.4(2)	
	27	21.52(4)	7.1(2)	
	31	0	0	
	100	0	0	-10.61(1)
10.1	12.6	36.25(6)	4.9(1)	
	15	35.31(6)	5.6(2)	
	20	32.96(5)	5.8(2)	
	23	31.82(8)	6.9(1)	
	26	30.28(6)	6.7(1)	
	30	28.49(5)	7.2(3)	
	34	25.74(6)	5.6(4)	
	36	24.48(8)	6.2(3)	
	38	23.3(2)	7.0(4)	
	46	16.7(1)	6.5(2)	
	52	0	0	
	100	0	0	-9.75(1)
15.4	13.5	40.73(5)	5.8(1)	
	15	40.11(8)	5.6(1)	
	18	38.36(8)	5.7(2)	
	21	36.25(9)	6.2(1)	
	35	0	0	
	100	0	0	-8.80(1)
17.1	13.4	44.43(6)	6.5(2)	
	16	43.1(1)	5.0(1)	
	19	41.2(1)	6.2(2)	
	35	0	0	
	100	0	0	-8.10(2)
20.5	13.5	49.0(1)	6.7(3)	
	16	47.1(1)	5.5(1)	
	33	0	0	
	100	0	0	-7.60(7)
25.2	13	9.85(4)	5.6(2)	
	40	0	0	
	100	0	0	-6.81(1)
27.1	13	0	0	
27.4	100	0	0	-5.80(2)

The results from SMS and PYF-XAS experiments are summarized in figure 6. Error in valence at each pressure from XAS data is from the fitting. T_o and error are estimated based

on two adjacent temperatures where $\text{Eu}(\text{Fe}_{0.75}\text{Ru}_{0.25})_2\text{As}_2$ was observed in the magnetic and paramagnetic phases at constant pressure. Based on the isomer shift values mean valence

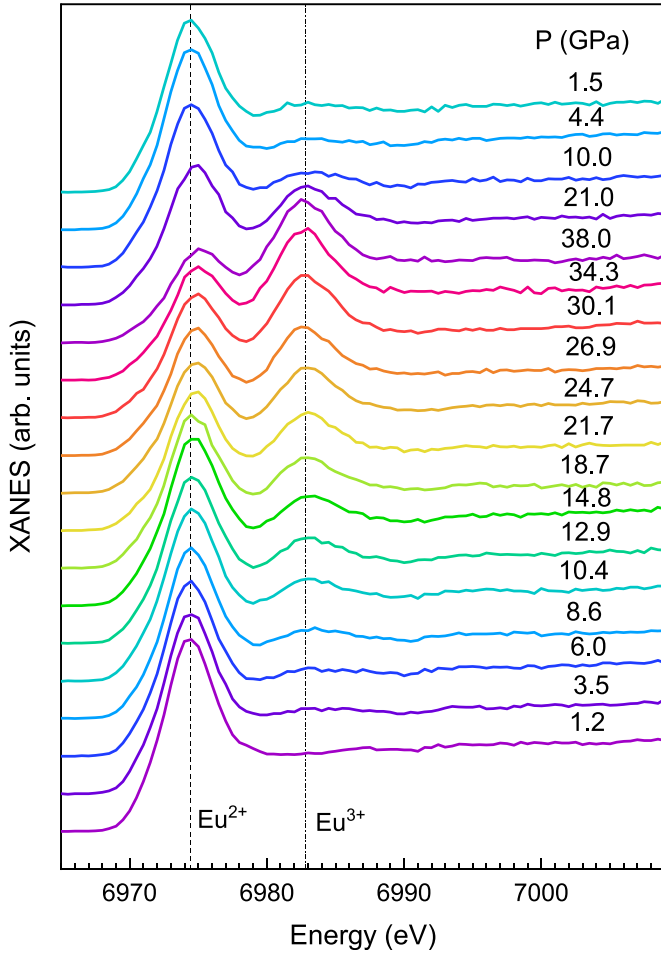


Figure 4. Selected PFY-XAS spectra at Eu L_3 edge in $\text{Eu}(\text{Fe}_{0.75}\text{Ru}_{0.25})_2\text{As}_2$ with increasing pressure from 1.2 GPa up to 38 GPa along with decompression data at 21, 10, 4.4, and 1.5 GPa. The two peaks at low and high energy are from Eu^{2+} and Eu^{3+} , respectively, with positions shown by the dash lines.

of Eu ions can also be estimated from linear extrapolation using -11.8 mm s^{-1} for Eu^{2+} and 0 mm s^{-1} for Eu^{3+} , assuming the changes in valence ($4f^7$ to $4f^6$) is entirely responsible for the pressure-induced changes in isomer shift. The pressure-induced valence changes derived from isomer shift and PYF-XAS measurements are in good agreement. Both methods conclude a monotonic increase in valence with pressure. An application of 38 GPa results in a mean valence of 2.6. Based on the linear dependence of valence with pressure, Eu ions are expected to fully transform to trivalent at around 63 GPa. The fact that the isomer shift data were taken at 100 K and PYF-XAS data were taken at room temperature shows insignificant impact of temperature on valence state of Eu in $\text{Eu}(\text{Fe}_{0.75}\text{Ru}_{0.25})_2\text{As}_2$. Despite of a slight increase of valence to ~ 2.2 , T_o increases initially up to 10.1 GPa, possibly due to pressure-enhanced RKKY exchange interactions. At higher pressure further increase of valence weakens the magnetic moment and leads to a decrease in T_o , which eventually suppresses the magnetic order above 25.2 GPa with a critical valence of ~ 2.4 . Interestingly, the parent compound EuFe_2As_2 demonstrates a similar initial increase of T_o with pressure and

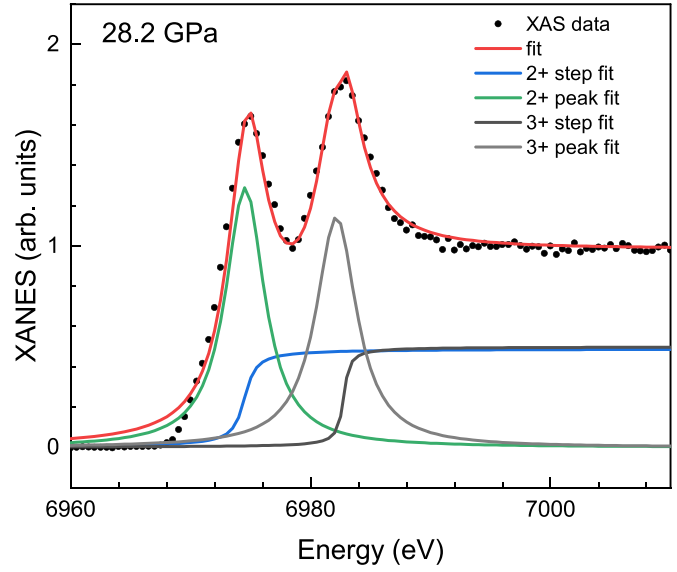


Figure 5. Analysis of PYF-XAS data at 28.2 GPa using two sets of Lorentzian and arctangent functions for Eu^{2+} and Eu^{3+} .

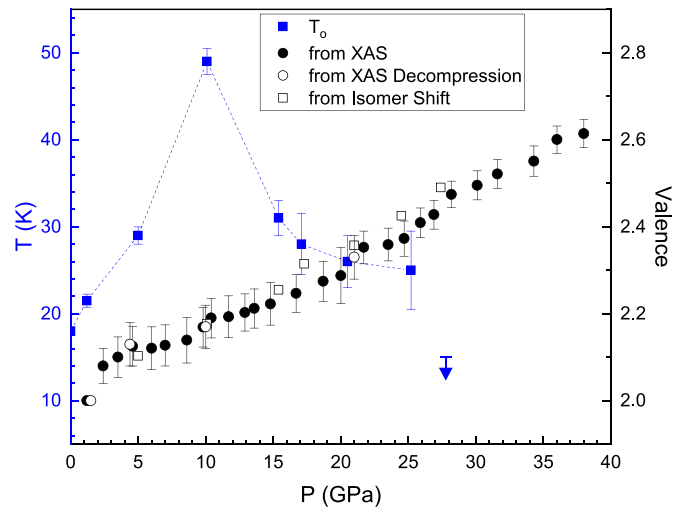


Figure 6. Evolution of magnetic ordering temperature and Eu mean valence under pressure in $\text{Eu}(\text{Fe}_{0.75}\text{Ru}_{0.25})_2\text{As}_2$. The blue arrow at 27.4 GPa indicates the absence of magnetic order at temperatures down to 13 K. The error bars are described in the text.

a subsequent suppression of magnetic order above 20 GPa that is related to the increase in valence of Eu ions [24, 44, 45].

3.3. XRD

To further compare with the parent compound, synchrotron XRD experiment were conducted to study possible crystal structural transition. Figure 7 summarizes the XRD data in $\text{Eu}(\text{Fe}_{0.75}\text{Ru}_{0.25})_2\text{As}_2$ from 4.4 to 12.4 GPa with ~ 1 GPa pressure step. The XRD patterns can be indexed with the tetragonal structure ($I4/mmm$). The lattice parameters and volume as a function of pressure are depicted in figure 8. The lattice parameter a first shows an anomalous increase up to 5 GPa followed by a normal compression behavior at higher

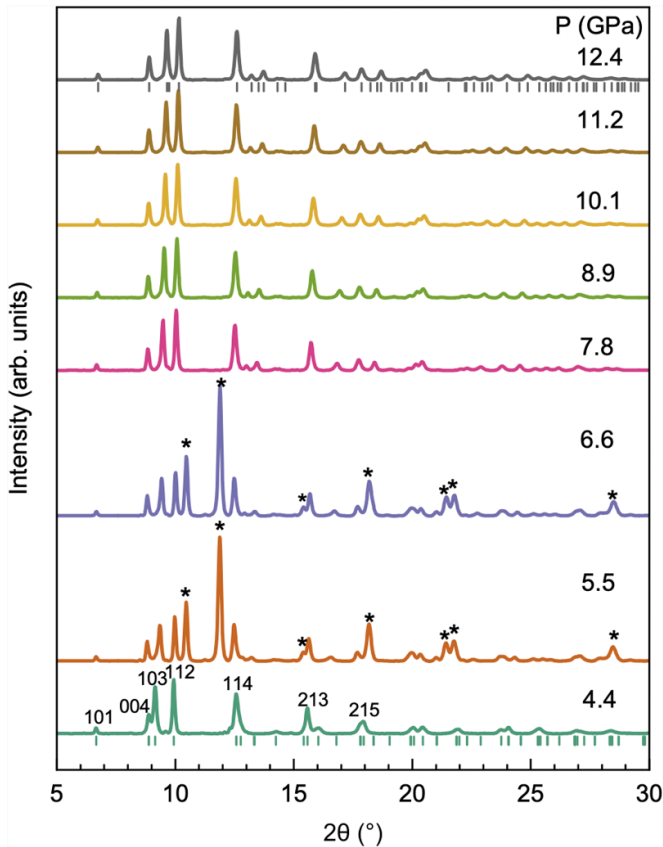


Figure 7. XRD spectra of $\text{Eu}(\text{Fe}_{0.75}\text{Ru}_{0.25})_2\text{As}_2$ taken at various pressures. Peaks from Re gasket are visible in the data at 5.5 and 6.6 GPa and indicated by asterisks. Tick marks show peak positions at 4.4 and 12.4 GPa based on the tetragonal structure with space group $I4/mmm$. At 4.4 GPa intense diffraction peaks are labeled with respective (hkl) Miller indices.

pressure, while parameter c initially decreases rapidly and above 5 GPa becomes less compressible (figures 8(a) and (b)). The axial ratio parameter c/a shows similar but more pronounced slope change with pressure (figure 8(c)). This behavior has also been observed in the parent compound EuFe_2As_2 above 8 GPa, attributed to a tetragonal to collapsed-tetragonal transition [46]. By comparing with the lattice behavior in EuFe_2As_2 , we conclude that in $\text{Eu}(\text{Fe}_{0.75}\text{Ru}_{0.25})_2\text{As}_2$ the tetragonal to collapsed-tetragonal transition occurs between 4.4 and 5.5 GPa, a lower pressure than in the parent compound.

$\text{Eu}(\text{Fe}_{0.75}\text{Ru}_{0.25})_2\text{As}_2$ and EuFe_2As_2 show similar high-pressure behaviors. With increasing pressure both systems show large increase in magnetic ordering temperature and subsequent suppression of magnetic order, valence transition, and tetragonal to collapsed-tetragonal transition. Difference in high-pressure behaviors has also been observed. In $\text{Eu}(\text{Fe}_{0.75}\text{Ru}_{0.25})_2\text{As}_2$ the magnetic ordering temperature increases monotonically with pressure up to 10.1 GPa, while in EuFe_2As_2 the magnetic ordering temperature is initially insensitive to the pressure change up to 2.5 GPa and only shows increase at higher pressure. In addition, the collapsed-tetragonal phase occurs at a lower pressure in $\text{Eu}(\text{Fe}_{0.75}\text{Ru}_{0.25})_2\text{As}_2$, which can be attributed to the chemical

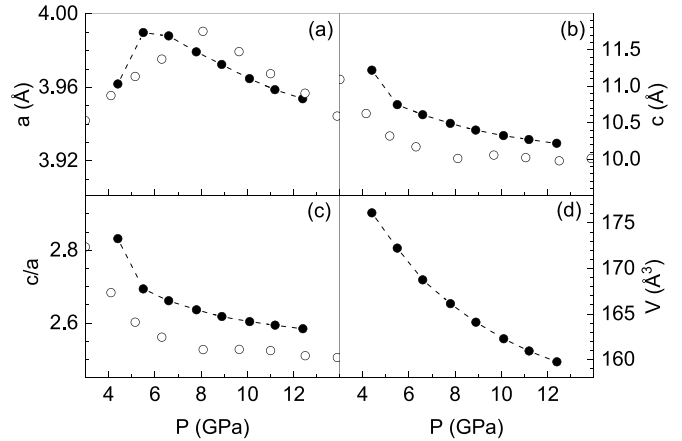


Figure 8. The measured lattice parameters a (a), c (b), axial ratio c/a (c), and volume (d) in $\text{Eu}(\text{Fe}_{0.75}\text{Ru}_{0.25})_2\text{As}_2$ as a function of pressure (solid circles). High pressure lattice data in EuFe_2As_2 from [46] are included (open circles) as a comparison.

pressure by Ru-substitution that yields a smaller lattice parameter c at ambient pressure.

4. Summary

We have studied the magnetic order, valence state, and crystal structure of $\text{Eu}(\text{Fe}_{0.75}\text{Ru}_{0.25})_2\text{As}_2$ under high pressure using synchrotron spectroscopy and diffraction techniques. Pressure effectively enhances the magnetic ordering T_o to ~ 49 K at 10.1 GPa from 20 K at ambient pressure. Further compression leads to a decrease in T_o . At 27.1 GPa no magnetic order is detected down to 13 K. A homogeneous valence transition from divalent to trivalent in Eu has been observed with increasing pressure and decompression data shows that this transition is reversible. The suppression of magnetism is likely associated with the significant valence increase. A tetragonal to collapsed-tetragonal transition around 5 GPa is concluded based on the anomalous changes in lattice parameters. Future studies of pressure effect on superconductivity are necessary to provide a complete understanding on the interplay of superconductivity, magnetism, and valence in this fascinating material.

Data availability statement

The data that support the findings of this study are available upon reasonable request from the authors.

Acknowledgments

This work was supported by the National Science Foundation (NSF) CAREER Award No. DMR-2045760. Z Nix acknowledges the support from the Department of Education-Graduate Assistantship in Areas of National Need (GAANN) Grant No. P200A180001. This research used resources of the Advanced Photon Source, a U.S. Department of Energy (DOE) Office of Science User Facility operated for the

DOE Office of Science by Argonne National Laboratory under Contract No. DE-AC02-06CH11357. HPCAT (High Pressure Collaborative Access Team) operations are supported by DOE-NNSA's (National Nuclear Security Administration) Office of Experimental Sciences. Support from the Consortium for Materials Properties Research in Earth Sciences (COMPRES) under NSF Cooperative Agreement EAR-1606856 is acknowledged for COMPRES-GSECARS gas loading system and the PX² program. We thank S Tkachev for help with the helium gas loading in diamond anvil cell. G-H C acknowledges the support from the National Key Research and Development Program of China (Grant No. 2016YFA0300202).

ORCID iDs

Guang-Han Cao  <https://orcid.org/0000-0002-9669-5761>
 Yogesh K Vohra  <https://orcid.org/0000-0002-2776-3695>
 Wenli Bi  <https://orcid.org/0000-0002-2067-6556>

References

- [1] Dai A, Kenji I and Jacques F 2019 Review of U-based ferromagnetic superconductors: comparison between UGe₂, URhGe and UCoGe *J. Phys. Soc. Japan* **88** 22001
- [2] Prozorov R, Vannette M D, Law S A, Bud'ko S L and Canfield P C 2008 Coexistence of ferromagnetism and superconductivity in ErRh₄B₄ single crystals probed by dynamic magnetic susceptibility *Phys. Rev. B* **77** 100503(R)
- [3] Fischer Ø, Treyvaud A, Chevrel R and Sergent M 1975 Superconductivity in the Re₇Mo₆S₈ *Solid State Commun.* **17** 721–4
- [4] Maiwald J and Gegenwart P 2016 Interplay of 4f and 3d moments in EuFe₂As₂ iron pnictides *Phys. Status Solidi b* **9** 1–9
- [5] Jackson D E et al 2018 Superconducting and magnetic phase diagram of RbEu₄As₄ and CsEuFe₄As₄ at high pressure *Phys. Rev. B* **98** 014518
- [6] Chenchao X, Chen Q and Cao C 2019 Unique crystal field splitting and multiband RKKY interactions in Ni-doped EuRbFe₄As₄ *Commun. Phys.* **2** 16
- [7] Albedah M A, Farshad Nejdassattari Z M Stadnik Y L and Cao G-H 2018 Mössbauer spectroscopy measurements on the 35.5 K superconductor Rb_{1-δ}EuFe₄As₄ *Phys. Rev. B* **97** 144426
- [8] Iida K et al 2019 Coexisting spin resonance and long-range magnetic order of Eu in EuRbFe₄As₄ *Phys. Rev. B* **100** 014506
- [9] Xiang Li, Bud'ko S L, Bao J-K, Chung D Y, Kanatzidis M G and Canfield P C 2019 Pressure-temperature phase diagram of the EuRbFe₄As₄ superconductor *Phys. Rev. B* **99** 144509
- [10] Ikeda S et al 2018 New antiferromagnetic order with pressure-induced superconductivity in EuFe₂As₂ *Phys. Rev. B* **98** 100502(R)
- [11] Si-Qi W, Wang Z-C, Chao-Yang H, Tang Z-T, Liu Y and Cao G-H 2017 Superconductivity at 33–37 K in AAn₂Fe₄As₄O₂ (A = Kand Cs; Ln = lanthanides) *Phys. Rev. Mater.* **1** 044804
- [12] Zapf S and Dressel M 2017 Europium-based iron pnictides: a unique laboratory for magnetism, superconductivity and structural effects *Rep. Prog. Phys.* **80** 016501
- [13] Liu Y, Liu Y-B, Ya-Long Y, Tao Q, Feng C-M and Cao G-H 2017 RbEu(Fe_{1-x}Ni_x)₄As₄: from a ferromagnetic superconductor to a superconducting ferromagnet *Phys. Rev. B* **96** 224510
- [14] Kawashima K et al 2018 Superconducting state in Eu_{1-x}Ca_xRbFe₄As₄ with 1144-type structure *J. Phys.: Conf. Ser.* **969** 012027
- [15] McGuire M A, Hermann Rel P, Sefat A S, Sales B C, Jin R, Mandrus D, Grandjean F and Long G J 2009 Influence of the rare-earth element on the effects of the structural and magnetic phase transitions in CeFeAsO, PrFeAsO and NdFeAsO *New J. Phys.* **11** 025011
- [16] Błachowski A, Ruebenbauer K, Żukrowski J, Bukowski Z, Rogacki K, Moll P J W and Karpinski J 2011 Interplay between magnetism and superconductivity in EuFe_{2-x}Co_xAs₂ studied by ⁵⁷Fe and ¹⁵¹Eu Mössbauer spectroscopy *Phys. Rev. B* **84** 174503
- [17] Nowik I, Felner I, Ren Z, Cao G H and Xu Z A 2011 ⁵⁷Fe and ¹⁵¹Eu Mössbauer spectroscopy and magnetization studies of Eu(Fe_{0.89}Co_{0.11})₂As₂ and Eu(Fe_{0.9}Ni_{0.1})₂As₂ *New J. Phys.* **13** 023033
- [18] Ren Z, Zhu Z, Jiang S, Xiangfan X, Tao Q, Wang C, Feng C, Cao G and Xu Z'an 2008 Antiferromagnetic transition in EuFe₂As₂: a possible parent compound for superconductors *Phys. Rev. B* **78** 052501
- [19] Jun Zhao W Ratcliff J W Lynn G F Chen J L Luo N L Wang J H and Dai P 2008 Spin and lattice structures of single-crystalline SrFe₂As₂ *Phys. Rev. B* **78** 140504(R)
- [20] Rotter M, Tegel M, Johrendt D, Schellenberg I, Hermes W and Rainer P 2008 Spin-density-wave anomaly at 140 K in the ternary iron arsenide BaFe₂As₂ *Phys. Rev. B* **78** 020503(R)
- [21] Terashima T, Kimata M, Satsukawa H, Harada A, Hazama K, Uji S, Suzuki H S, Matsumoto T and Murata K 2009 EuFe₂As₂ under high pressure: an antiferromagnetic bulk superconductor *J. Phys. Soc. Japan* **78** 083701
- [22] Kurita N, Kimata M, Kodama K, Harada A, Megumi Tomita H S Suzuki T M, Murata K, Uji S and Terashima T 2011 Phase diagram of pressure-induced superconductivity in EuFe₂As₂ probed by high-pressure resistivity up to 3.2 GPa *Phys. Rev. B* **83** 214513
- [23] Miclea C F, Nicklas M, Jeevan H S, Kasinathan D, Hossain Z, Rosner H, Gegenwart P, Geibel C and Steglich F 2009 Evidence for a reentrant superconducting state in EuFe₂As₂ under pressure *Phys. Rev. B* **79** 212509
- [24] Matsubayashi K et al 2011 Pressure-induced changes in the magnetic and valence state of EuFe₂As₂ *Phys. Rev. B* **84** 024502
- [25] Uhoya W O, Tsoi G M, Vohra Y K, McGuire M A and Sefat A S 2011 Structural phase transitions in EuFe₂As₂ superconductor at low temperatures and high pressures *J. Phys.: Condens. Matter* **23** 365703
- [26] Onuki Y et al 2017 Divalent, trivalent and heavy fermion states in Eu compounds *Phil. Mag.* **97** 3399–414
- [27] Hesse H J, Lübbers R, Winzenick M, Neuling H W and Wortmann G 1997 Pressure and temperature dependence of the Eu valence in EuNi₂Ge₂ and related systems studied by Mössbauer effect, X-ray absorption and X-ray diffraction *J. Alloys Compd.* **246** 220–31
- [28] Chunyu Li et al 2016 High-pressure synchrotron Mössbauer and X-ray diffraction studies: Exploring the structure-related valence fluctuation in EuNi₂P₂ *Physica B* **501** 101–5
- [29] Jiao W-H, Tao Q, Bao J-K, Sun Y-L, Feng C-M, Zhu-An X, I Felner N, I and Cao G-H 2011 Anisotropic superconductivity in Eu(Fe_{0.75}Ru_{0.25})₂As₂ ferromagnetic superconductor *Europhys. Lett.* **95** 67007
- [30] Zhou Z et al 2019 Universal critical behavior in the ferromagnetic superconductor Eu(Fe_{0.75}Ru_{0.25})₂As₂ *Phys. Rev. B* **100** 060406

- [31] Bi W *et al* 2012 Synchrotron x-ray spectroscopy studies of valence and magnetic state in europium metal to extreme pressures *Phys. Rev. B* **85** 205134
- [32] Sergueev I *et al* 2013 Hyperfine splitting and room-temperature ferromagnetism of Ni at multimegabar pressure *Phys. Rev. Lett.* **111** 157601
- [33] Bi W *et al* 2016 Magnetism of europium under extreme pressures *Phys. Rev. B* **93** 184424
- [34] Wenli B *et al* 2021 Microscopic phase diagram of $\text{Eu}(\text{Fe}_{1-x}\text{Ni}_x)\text{As}_2$ ($x = 0, 0.04$) under pressure *Phys. Rev. B* **103** 195135
- [35] Zhao J Y, Bi W, Sinogeikin S, Hu M Y, Alp E E, Wang X C, Jin C Q and Lin J F 2017 A compact membrane-driven diamond anvil cell and cryostat system for nuclear resonant scattering at high pressure and low temperature *Rev. Sci. Instrum.* **88** 125109
- [36] Dewaele Aès, Torrent M, Loubeyre P and Mezouar M 2008 Compression curves of transition metals in the Mbar range: experiments and projector augmented-wave calculations *Phys. Rev. B* **78** 104102
- [37] Sturhahn W 2000 CONUSS and PHOENIX: Evaluation of nuclear resonant scattering data *Hyperfine Interact.* **125** 149–72
- [38] Ravel B and Newville M 2005 ATHENA, ARTEMIS, HEPHAESTUS: data analysis for X-ray absorption spectroscopy using IFEFFIT *J. Synchrotron Radiat.* **12** 537–41
- [39] Kantor I, Prakapenka V, Kantor A, Dera P, Kurnosov A, Sinogeikin S, Dubrovinskaia N and Dubrovinsky L 2012 BX90: a new diamond anvil cell design for X-ray diffraction and optical measurements *Rev. Sci. Instrum.* **83** 125102
- [40] Prescher C and Prakapenka V B 2015 DIOPTAS : a program for reduction of two-dimensional X-ray diffraction data and data exploration *High Press. Res.* **35** 223–30
- [41] Toby B H and Von Dreele R B 2013 GSAS-II : the genesis of a modern open-source all purpose crystallography software package *J. Appl. Crystallogr.* **46** 544–9
- [42] Perscheid B, Nowik I, Wortmann G, Schmiester G, Kaindl G and Felner I 1989 Eu valency and recoil-free fraction in $\text{EuCo}_2\text{Si}_{2-x}\text{Ge}_x$ *Z. Phys. B* **73** 511–7
- [43] Padalia B D, Prabhawalkar V, Prabhawalkar P D, Sampathkumaran E V, Gupta L C and Vijayaraghavan R 1981 ESCA studies of some mixed-valence rare-earth intermetallics *Bull. Mater. Sci.* **3** 163–7
- [44] Sun L *et al* 2010 Valence change of europium in $\text{EuFe}_2\text{As}_{1.4}\text{P}_{0.6}$ and compressed EuFe_2As_2 and its relation to superconductivity *Phys. Rev. B* **82** 134509
- [45] Kumar R S, Zhang Y, Thamizhavel A, Svane A, Vaitheeswaran G, Kanchana V, Xiao Y, Chow P, Chen C and Zhao Y 2014 Pressure induced valence change of Eu in EuFe_2As_2 at low temperature and high pressures probed by resonant inelastic x-ray scattering *Appl. Phys. Lett.* **104** 042601
- [46] Uhoya W *et al* 2010 Anomalous compressibility effects and superconductivity of EuFe_2As_2 under high pressures *J. Phys.: Condens. Matter* **22** 292202